AGU PUBLICATIONS

Geophysical Research Letters

RESEARCH LETTER
10.1002/2014GL060956

Key Points:
- We use PS-InSAR method to detect volcanic deformation at Tungurahua volcano
- We measure large-scale and long-term inflation at Tungurahua volcano
- We model the deformation and estimate magma emplacement and inflation rate

Supporting Information:
- Readme
- Text S1
- Figure S2
- Figure S3
- Figure S4

Correspondence to:
J. Champenois,
johann.champenois@irsn.fr

Citation:
Champenois, J., V. Pinel, S. Baize, L. Audin, H. Jomard, A. Hooper, A. Alvarado, and H. Yepes (2014), Large-scale inflation of Tungurahua volcano (Ecuador) revealed by Persistent Scatterers SAR interferometry, *Geophys. Res. Lett.*, *41*, 5821–5828, doi:10.1002/2014GL060956.

Received 19 JUN 2016
Accepted 1 AUG 2014
Accepted article online 4 AUG 2014
Published online 20 AUG 2014

Large-scale inflation of Tungurahua volcano (Ecuador) revealed by Persistent Scatterers SAR interferometry

J. Champenois[1,2], V. Pinel[2], S. Baize[1], L. Audin[2], H. Jomard[1], A. Hooper[3], A. Alvarado[4], and H. Yepes[2,4]

[1]Institut de Radioprotection et de Sûreté Nucléaire, Fontenay-aux-Roses, France, [2]Institut des Sciences de la Terre UMR 5275, Grenoble, France, [3]COMET+, School of Earth and Environment, University of Leeds, Leeds, UK, [4]Instituto Geofísico, Escuela Politécnica Nacional, Quito, Ecuador

Abstract The Tungurahua volcano, in Ecuador, has been experiencing a substantial activity period since 1999, with several eruptions, including those of 2006 and 2008. We use a persistent scatterers approach to analyze a time series of Envisat synthetic aperture radar (SAR) data over the period 2003–2009, to investigate surface deformation in the region of the volcano. We measure a continuous large-scale uplift with a maximum line of sight displacement rate of about 8 mm/yr, which is the first evidence of a sustained inflation in the Andes for an active volcano encompassing several eruptions. We model this signal as magma emplacement in a permanent storage zone at 11.5 km below sea level, with a net inflow rate of 7 million m^3/yr. The paroxysmal eruptions in 2006 and 2008 did not seem to disrupt this long-term signal. However, we observe significant deformation during the 2006 eruption consistent with an additional intrusion of 4.5 million m^3 of magma.

1. Introduction

Synthetic aperture radar interferometry (InSAR) can provide maps of surface displacements over large areas with an accuracy reaching a few mm/yr over tens of kilometers. As a remote technique, it does not require any specific field instrumentations and has early been identified as a valuable method to detect and follow surface deformations around volcanoes [*Dzurisin*, 2003; *Hooper et al.*, 2012a]. The main limitations of this technique are due to spatiotemporal decorrelation and atmospheric perturbations to interferometric phase [*Zebker and Villasenor*, 1992], which makes the application of InSAR to andesitic stratocones challenging [*Pinel et al.*, 2011]. However, the signal-to-noise ratio can be significantly increased by Multitemporal InSAR (MT-InSAR) techniques based on the processing of multiple synthetic aperture radar (SAR) acquisitions in time [*Hooper et al.*, 2012b].

Allowing for regional studies, InSAR has been widely applied to the Andes volcanic arc. *Pritchard and Simons* [2002] first focused on the Central Andes and detected two uplifting areas around currently inactive volcanoes: Uturuncu (22.27°S, 67.22°W) and Lazufre (25.25°S, 68.49°W), where inflation has later been shown to last for more than 10 years [*Froger et al.*, 2007; *Sparks et al.*, 2008; *Fournier et al.*, 2010; *Fialko and Pearse*, 2012; *Henderson and Pritchard*, 2013; *Walter and Motagh*, 2014]. At Uturuncu volcano, an uplift of around 1–2 cm/yr over 70 km was recorded from 1992 to 2011, which has been interpreted as being due to magma emplacement at 17 to 24 km depth at a rate of 10–29 million m^3/yr [*Sparks et al.*, 2008; *Henderson and Pritchard*, 2013]. Based on the observation of a ring of subsidence around the uplifting area, *Fialko and Pearse* [2012] propose that this signal of deformation could be produced by a diapir of magma rising from the Altiplano-Puna Magma Body, a large midcrustal melt zone. At Lazufre (also known as Lastarria-Cordon del Azufre volcanic complex), the uplift recorded since 1996 is around 2–3.5 cm/yr over 40 km and corresponds to a slightly shallower source (7–15 km) with a rate of magma emplacement of 14–17 million m^3/yr [*Froger et al.*, 2007; *Henderson and Pritchard*, 2013]. Such long-term inflating zones, which imply large storage of magma within the crust, have significant consequences in terms of risk assessment, with the linked question of the future evolution of these storage zones and the potential risk of a large silicic eruption [*Sparks et al.*, 2008]. Using L-band data, *Fournier et al.* [2010] and *Feigl et al.* [2014] extended the application of InSAR to the Southern Andes and Northern Andes detecting uplift at several currently nonactive volcanoes, including Cordon Caulle and Laguna del Maule. Inflation was also observed, for at least 6 years, before the 2011 eruption of Cerro Hudson [*Delgado et al.*, 2014]. Coeruptive subsidence was measured using L-band data at Galeras, Colombia [*Parks et al.*, 2011]. Other deformation signals inferred at Andean volcanoes have

been based on a few ground measurements (tiltmeters, leveling, and GPS) [*Ordóñez and Rey*, 1997; *Mothes et al.*, 2010].

In the Northern Andes, Ecuador encompasses one of the most active volcanic areas. With presently nine active volcanoes including three currently erupting (Reventador, Tungurahua, and Sangay), volcanic hazard assessment is a crucial issue in this country and the enhancement of volcano monitoring requires dense ground measurements. For the last 5 years, GPS networks have been deployed over the main hazardous volcanoes in Ecuador, but these pointwise measurements cannot provide spatially dense maps of ground deformation.

In this study, we use InSAR to dramatically increase the density of measurements around Tungurahua volcano, which is currently the most active volcano in Ecuador. Over the period 1992–2002, the ERS data available were sparse in time and affected by strong decorrelation over the Tungurahua [*Stevens and Wadge*, 2004]. Previous studies [*Biggs et al.*, 2010; *Fournier et al.*, 2010] based on Phased Array type L-band SAR images provided by the Advanced Land Observing Satellite (L-band) showed a rapid uplift of Tungurahua during the 2008 eruption and inferred a sill-like magmatic source located at shallow depth within the volcanic edifice. Their estimated volume for the sill of 1.2 million m^3 was almost equivalent to the volume of magma erupted in February 2008. We present results from advanced synthetic aperture radar (ASAR) data provided by the Envisat satellite (C-band with a 5.6 cm wavelength) acquired between 2003 and 2009, covering the two major phases of the ongoing Tungurahua activity in 2006 and 2008. Moreover, we applied the Persistent Scatterers InSAR (PSI) technique in order to perform a proper time series analysis of ground deformation induced by magma intrusion during eruptive cycle. We then modeled the resulting signal using an analytical solution for a point pressure source [*Mogi*, 1958] and a numerical model.

2. Tungurahua Recent Eruptive Activity

Tungurahua volcano (reaching 5023 m above sea level) is an andesitic stratovolcano located in the Eastern Cordillera of Ecuador. This steep-sided edifice (12 km in diameter) is surrounded by two other potentially active volcanoes (Chimborazo and Puñalica) and numerous inactive volcanic edifices (Figure 1). Based on geologic studies, Tungurahua's eruptive rate has been estimated to be around 1.5 million m^3/yr dense rock equivalent (DRE) of magma over the last 2300 years [*Hall et al.*, 1999]. Tungurahua has had five main eruptive periods during historical time: 1640–1641, 1773–1777, 1886–1888, 1916–1918, and 1999 to present [*Hall et al.*, 1999; *Ruiz et al.*, 2006; *Le Pennec et al.*, 2008]. After more than 80 years of repose, on 5 October 1999, Tungurahua began the current eruptive cycle, characterized by intermittent strombolian eruptions and punctuated by significant vulcanian to subplinian eruptions [*Ruiz et al.*, 2006; *Samaniego et al.*, 2011].

The volcanic edifice is monitored by a national seismic network, which has been operated by the Instituto Geofísico, Escuela Politécnica Nacional of Ecuador since 1993. Volcano-tectonic earthquakes recorded by this network have been used to produce a tomographic study of the upper 5 km of crust beneath the volcano, showing a shallow and vertical magma body which feeds the system [*Molina et al.*, 2005]. In early April 2006, the Tungurahua Volcanological Observatory observed deep long-lasting seismic activity (5–15 km below the summit). The seismic activity dramatically increased until the beginning of July 2006 and peaked during the 14 July and 16–17 August eruptions (apps.igepn.edu.ec/cnd). The 2006 eruptions were characterized by highly explosive events associated with pyroclastic flows, affecting the western flank of the volcano [*Samaniego et al.*, 2011], which caused about five to six fatalities and destroyed villages. The 14 July eruption was a moderate-size event, Volcanic Explosive Index (VEI) 2, with the emission of about 1 million m^3 DRE, whereas the 16–17 August eruption reached VEI 3 with an eruptive column height around 16 km above the vent [*Eychenne et al.*, 2012]. During this eruptive event, 30 Pyroclastic density currents with an estimated volume of 18.7 million m^3 DRE [*Hall et al.*, 2013] were emplaced together with a DRE volume of juvenile tephra of 7.7 million m^3 [*Eychenne et al.*, 2013]. The explosive phase was followed by lava flow with an estimated volume of 7 million m^3 [*Arellano et al.*, 2008; *Hall et al.*, 2013]. The total volume of magma emitted during the August 2006 eruption is thus estimated to be 30 million m^3 DRE. From October 2006 to the next paroxysmal eruptive phase in early 2008, the Tungurahua activity returned to an eruptive cycle similar to the 1999–2005 period. This last 2008 paroxysmal phase was characterized by the emission of a much lower quantity of magma of about 1.5 million m^3 [*Biggs et al.*, 2010] in comparison to the major 2006 event.

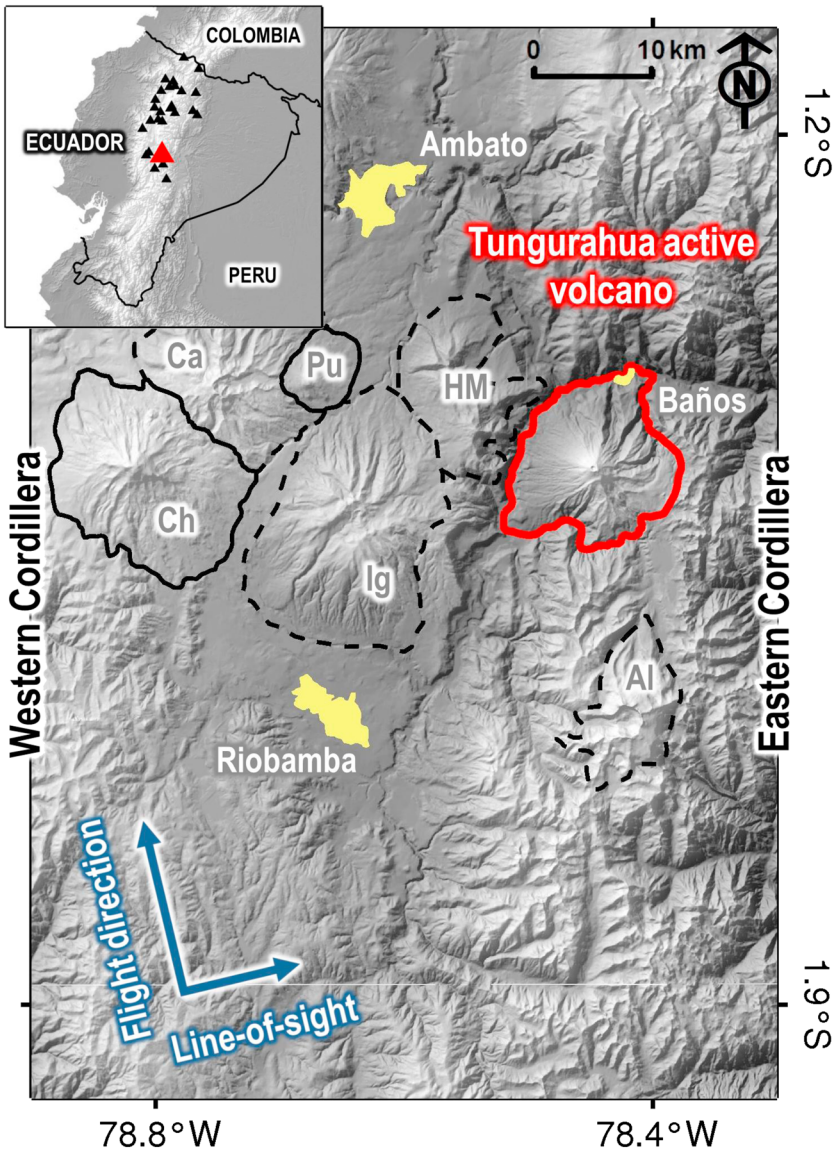

Figure 1. Shaded relief map of the volcanic zone surrounding the Tungurahua active volcano (red line). Black lines represent volcanoes with activity in the last thousand years (Ch: Chimborazo; Pu: Puñalica) while black dashed lines represent extinct volcanoes (Al: Cerro Altar; Ca: Carihuairazo; HM: Huisla and Mulmul; Ig: Igualata). Yellow polygons indicate major urban areas. The blue arrows in the lower left corner show the ascending flight direction of the satellite and the look direction of the radar. Inset: Location map of the Tungurahua volcano in the Ecuadorean Andes.

3. InSAR Persistent Scatterers Measurements

3.1. Method and Data

The Stanford Method for Persistent Scatterers (StaMPS) developed by *Hooper et al.* [2007] was applied to 22 Envisat images acquired over the Tungurahua volcano between July 2003 and June 2009 (Text S1 in the supporting information for processing parameters). This PS (Persistent Scatterers) approach uses both information of amplitude dispersion [*Ferretti et al.*, 2001] and phase stability with time to select PS pixels. During the phase analysis, the probability for a pixel to be a PS is estimated and refined through a series of iterations. Starting from SAR raw data, 21 interferograms were calculated with 14 April 2006 as the common master image using ROI_PAC [*Rosen et al.*, 2004] and Doris software. Interferograms were flattened and georeferenced using the 90 m resolution Shuttle Radar Topography Mission (SRTM) digital elevation model (DEM) [*Farr et al.*, 2007]. At the end of the StaMPS processing, a map of mean velocity along the radar line of sight (LOS velocity) is produced together with the displacement time series at each acquisition date for selected pixels.

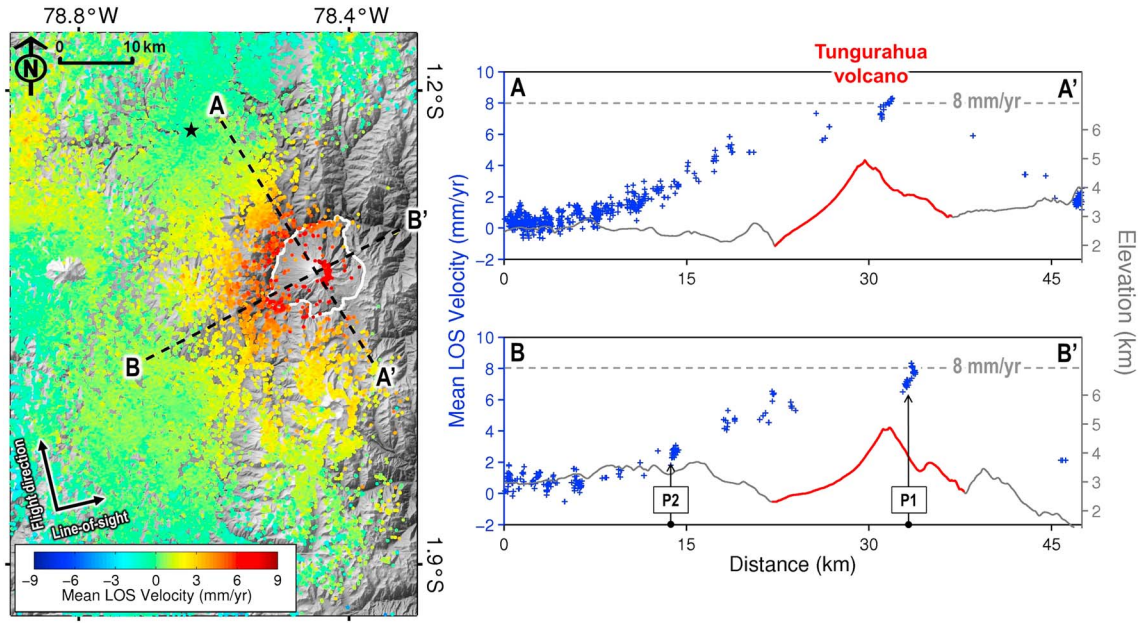

Figure 2. PS mean velocity map of Tungurahua volcano between July 2003 and June 2009 derived from Envisat SAR images. The velocities are relative to the mean LOS velocity of PS pixels of the reference area represented by the black star (Ambato city). The white line corresponds to the Tungurahua active volcano while black dashed lines indicate the location of the PS profiles. The black arrows in the lower left corner show the ascending flight direction of the satellite and the look direction of the radar (with a 23° look angle). The black dashed lines indicate the location of two PS profiles across the Tungurahua volcano superimposed on topographic profiles from the 90 m resolution SRTM digital elevation model where red lines show the Tungurahua topographic footprint. The black arrow on the lower right profile shows location of PS pixels used in Figure 3b.

3.2. Results

The mean LOS velocity map (Figure 2) for the period 2003–2009 was calculated for more than 190,000 PS pixels with a spatial density superior to 25 PS per km^2. LOS velocities are given with respect to the reference area which is located in the city of Ambato (see Figure 1 for location). The PS distribution is not homogeneous across the obtained map, with two main distinct areas: (i) the eastern cordillera with a low PS density (~10 PS per km^2) due to tropical vegetation that leads to radar phase instability, and (ii) the remaining area with an impressive PS density (~42 PS per km^2) due to the presence of man-made structures and large rock outcrops. Uncertainties in the mean LOS velocities are estimated by the percentile bootstrap method [*Efron and Tibshirani*, 1986] and range from 0.3 mm/yr to 1.5 mm/yr (about 1.2 mm/yr in the area of the volcano, Figure S2). The very low standard deviations correspond to PS close to the reference area (Ambato city) and values increase with distance away from the reference due to increasing differences in the path delay through the atmosphere. Concerning the phase unwrapping, visible inspection of the wrapped phase (minus DEM error and master atmosphere) shows no jump in the unwrapped result, but we cannot categorically state that there is not a phase discontinuity surrounding the pixels on the eastern side.

The ground displacements clearly highlight a large circular pattern in the LOS velocity centered on the Tungurahua active volcanic complex. This pattern also includes surrounding areas, for instance, the eastern flank of the Igualata volcano and the city of Baños. The total affected area covers a zone of 25 km radius around the Tungurahua volcano. In contrast, the rest of the studied area displays much lower rates of deformation, with LOS velocities ranging between −2 mm/yr and 2 mm/yr. The two PS profiles across the Tungurahua volcano (Figure 2) show a highly symmetrical pattern of deformation, with a maximum LOS velocity of about 8.2 mm/yr, near the summit of the volcano. Incidentally, few PS are located on the active volcanic edifice (~450 pixels) mostly due to the ash deposits and lava flows of the 14 July and 16–17 August 2006 eruptions, as mapped by *Samaniego et al.* [2011].

The time series of LOS displacement between July 2003 and June 2009 calculated from the PS phases is presented in Figure 3a. Even though uplift of Tungurahua is approximately constant with time, the time series of LOS displacement for selected pixels located on the eastern summit of Tungurahua and western flank of Igualata (respectively, P1 and P2 in Figure 3b) indicates that deformation can be divided into three periods: (i) A steady uplift between 4 July 2003 and 10 March 2006, (ii) an increased uplift detected between

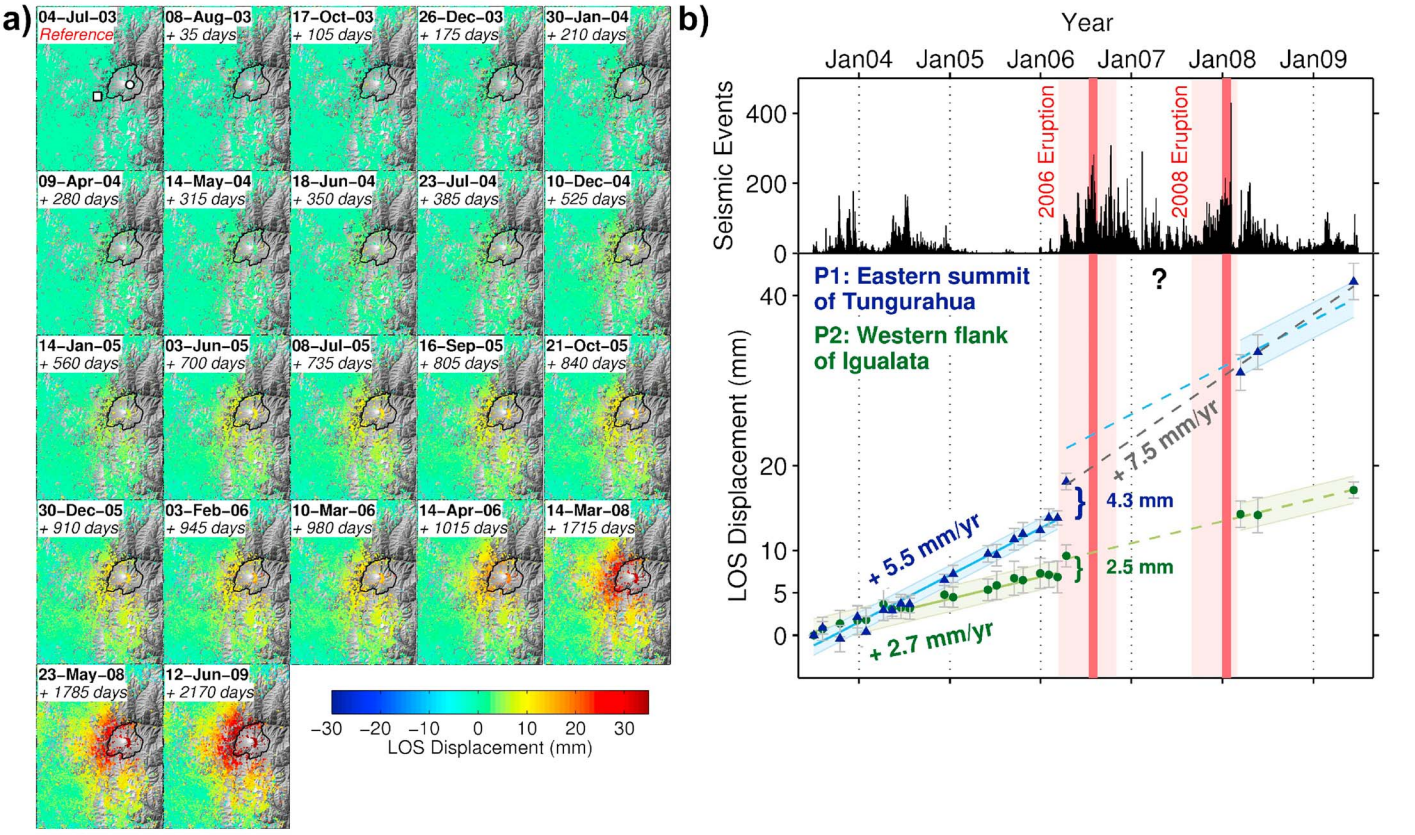

Figure 3. (a) The July 2003 to June 2009 time series of LOS displacement relative to the first image (in millimeters). White square and dot represent, respectively, P1 and P2 areas. (b) Average time series of LOS displacement of near- and far-field areas (see Figures 2 and 3a for exact location) associated to seismic activity (daily solutions from apps.igepn.edu.ec/cnd). The light red areas are for the high volcano-tectonic activity while dark red areas are for paroxysmal volcanic events associated to pyroclastic flows activity occurring during the study period. Blue and green lines represent the linear fits estimated for the long-term inflation while the grey line represents the near-field inflation rate after 2008.

10 March and 14 April 2006 (35 days), and (iii) a new steady period of uplift from March 2008 to June 2009, which appears to be similar or slightly larger than that experienced before the 2006 eruption. However, the latter is not well constrained, with only three measurements. Regarding P2, which is about 16 km to the west of the summit (far-field deformation), it is clear that the uplift rate is constant during the intereruptive periods (before March 2006 and after March 2008). On the other hand, the uplift rate of P1 after March 2008 is more questionable and two scenarios are possible: (i) the uplift rate is the same as before March 2006 and an additional uplift (+4.3 mm) occurs between April 2006 and March 2008 (blue curve in Figure 3b), and (ii) the uplift rate increases from 5.5 mm/yr to 7.5 mm/yr after the 2006 eruption (grey curve in Figure 3b). Note that these two scenarios fit equally well with the three last measurements available.

4. Deformation Source Modeling

To a first approximation, we considered the intereruptive inflation rate as constant, and modeled it using the classical analytical model derived by *Mogi* [1958] for a pressure point source in an elastic half-space. The best fitting model was obtained for a source at 1.47°S, 78.465°W located 14.5 km beneath the free surface, and characterized by a volume increase rate of 6.7 million m^3/yr. The residual root-mean-square error (RMSE) is 0.80 mm/yr (Figure S3). In order to account for the topography around the volcano, we also performed an inversion using a numerical model with the SRTM DEM as an input for the surface elevation. The surface displacements induced by a spherical source have been calculated using the 3-D finite element commercial Software COMSOL. We used a 100 × 100 × 50 km box containing 100,000 elements with a refined mesh at the surface and around the spherical magma reservoir. A "roller" condition (no displacement perpendicular to the surface) was applied on the lateral side and bottom frontiers (using infinite elements in order to artificially increase the numerical box size). The upper boundary (i.e., the volcano flank) was considered as a free

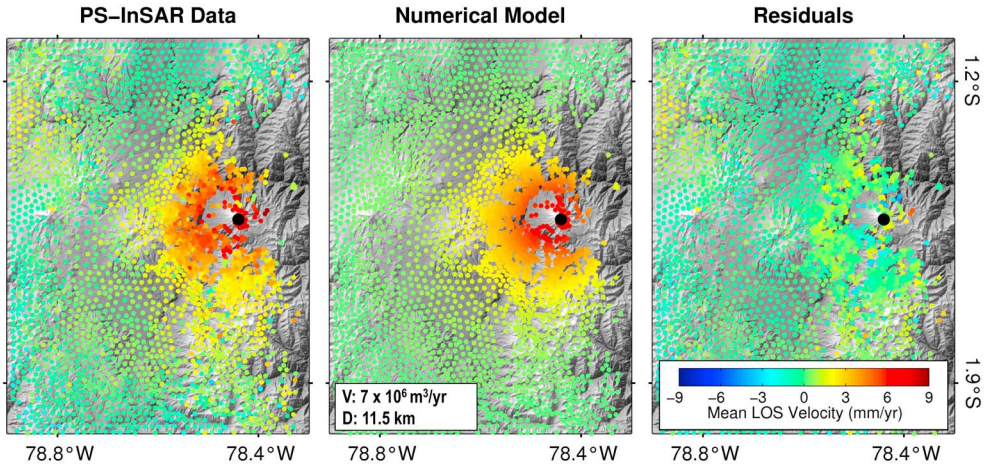

Figure 4. Mean LOS velocity at Tungurahua for the intereruptive period (before March 2006 and after February 2008) from (left) ascending PSI data, (middle) numerical model, and (right) residuals between data and model. The model was generated numerically for a spherical pressure source located below the topographic surface provided by the SRTM DEM. The black dot represents the projected center of the sphere used in the model. Best fitting model parameters are presented in the white box: volumetric change of the sphere (*V*) and depth of the sphere below sea level (*D*).

limit. A uniform surface displacement corresponding to a given volume increase was applied to the boundary of a spherical magma reservoir characterized by its location (latitude, longitude) and depth below sea level. Surface displacements were calculated for 4429 points, projected into the line of sight direction, and then compared with PS measurements. The best fitting model was obtained for a source located slightly eastward in comparison to the Mogi solution (1.475°S, 78.44°W) and at 11.5 km below sea level, with a volume increase rate of 7 million m^3/yr (see Figure 4). The residual RMSE is 0.79 mm/yr (Figure S4).

5. Discussion and Conclusions

Such a large-scale (25 km in radius) and long-term (over 6 years) inflation, as we measure around the Tungurahua volcano, has not been observed before in Ecuador. This is also the first time that a long-term inflation signal has been observed in the Andes for a volcano marked by several eruptions. The time series of LOS displacements covers both intereruptive and coeruptive periods of the volcanic cycle. The first intereruptive period, before March 2006, is well constrained by 18 measurements and is characterized by a constant inflation rate. The second intereruptive period, after March 2008, is less well constrained with only three measurements available. During this period, the far-field inflation rate is not affected by the eruptive periods while the near-field displacement appears less constant in time. However, the apparent change in the inflation rate is small enough, with respect to the measurement error, that it can be considered as constant during both intereruptive periods (blue curve in Figure 3b). The consistent behavior in near and far field is then well explained by a single-storage zone. The intereruptive constant inflation can be interpreted as being due to magma emplacement at 11.5 km depth below sea level with a mean intruded volume of about 7 million m^3/yr. The difference in RMSE between the analytical Mogi model and the numerical model is not significant, but the latter, taking into account the real topography, provides a more realistic estimation of the source depth. This model of a single-storage zone located at 11.5 km depth below sea level is in fairly good agreement with petrological data indicating an equilibration of the andesitic magma at 200 to 250 MPa corresponding to a depth of 7.5 to 9.5 km below the mean elevation of the area [*Samaniego et al.*, 2011]. However, if the inflation rate after 2008 in the near field is effectively slightly larger than before 2006 (grey curve in Figure 3b), the storage zone located at 11.5 km depth still explains most of the observed uplift but an additional storage zone is required at shallower level in order to explain a different temporal evolution in the near field and the far field. The presence of a shallow magma reservoir (around 5 km depth) and located on the same vertical path as a deeper midcrustal magma reservoir appears to be a common feature as it has been inferred at several other locations, including Montserrat, Fernandina, and Grimsvötn [*Elsworth et al.*, 2008; *Foroozan et al.*, 2010; *Bagnardi and Amelung*, 2012; *Reverso et al.*, 2014]. A withdrawal of the shallower reservoir by summit eruptions could induce an increase in its replenishment rate after these events and explain the inflation rate increase after the large 2006 eruption.

In addition to the long-term inflation rate, the time series of LOS displacement is marked by at least one significant offset in inflation, which occurred at the time of increased eruptive activity. This offset observed in both the far-field and near-field between March 2006 and April 2006 coincided with the deep long-period seismic activity monitored by the Tungurahua Volcanological Observatory. This offset in inflation together with the seismicity recorded can be interpreted as a larger-than-usual volume of magma migrating upward and inducing seismicity around the inferred storage zone between 10 and 15 km depth. Assuming a source depth similar to the one inferred for the intereruptive period, the volume of magma intruded would be around 4.5 million m^3. This sudden increase of magma supply to the storage zone is consistent with the sudden magma input shown by petrological data just prior to the 2006 eruption [*Samaniego et al.*, 2011; *Eychenne et al.*, 2013]. A shallower zone would imply a smaller volume of stored magma, and there is evidence of magma emplacement at a much shallower depth within this period of time. *Biggs et al.* [2010] show 17.5 cm of uplift on the upper western flank between 26 December 2007 and 27 March 2008, which they modeled with a sill-like magmatic source located at shallow depth within the volcanic edifice. Unfortunately, no PS pixels are identified over this part of the volcano to corroborate these previous results, presumably due to decorrelation caused by eruptive deposits [*Kelfoun et al.*, 2009; *Samaniego et al.*, 2011].

The mean rate of magma supply at depth obtained in this study is 4 times higher than the geologic estimation for eruptive deposits from *Hall et al.* [1999], which is about 1.5 million m^3/yr DRE. Integrating our estimated magma supply rate over the 6 year window of observations, and adding the additional amount of magma inflow that occurred just before the 2006 eruption, we obtain an intrusive volume of magma around 46.5 million m^3. We should also add the intrusive volume emplaced at shallow level, which is not constrained by our data set but has been estimated at 1.2 million m^3 during the 2008 eruption by *Biggs et al.* [2010]. The total intrusive volume is therefore slightly larger than the erupted volume of magma over the same time period (around 30 million m^3). It would suggest that the Tungurahua volcanic plumbing system and edifice grow by intrusion of magma at depth together with emplacement of eruptive products at the surface, both mechanisms accounting approximately for the same amount with a slightly larger part for intrusive growth. However, the intrusive rate might be underestimated due to magma compressibility [*Rivalta and Segall*, 2008] as suggested by the SO_2 emission measurements showing a larger amount of degassed magma than the erupted volume by 2 orders of magnitude [*Arellano et al.*, 2008]. Our study adds a further constraint on the intrusive/extrusive ratio at andesitic volcanoes, which was estimated, with large uncertainties, to be between 1 and 6 in the Andes, based on field observations of plutonic and volcanic provinces [*Crisp*, 1984]. However, a 6 year time window is short, and longer series of SAR observations would provide improved constraints on internal/external volcanic edifice growth. Another important inference of the almost constant deformation rate observed is that the deep magma supply rate is not significantly influenced by the eruptive activity; the volume of magma stored at depth is not modified by eruption or intrusion of magma at very shallow levels, supporting the idea that the magma erupted is compensated at depth by an acceleration of magma input. To our knowledge, this is the first example of constant net inflow of magma at depth below a currently active andesitic stratovolcano; other examples of long-term magma emplacement in the Andes occurring at volcanoes (Lazufre and Uturuncu). It raises question of the potential evolution of this large volume of magma and its ability to feed eruptions of larger volume in the future. The integration of ground-based measurements would also be helpful in adding further information, particularly on the volcanic edifice.

Our InSAR results provide a high-density map of measurements, enabling us to constrain the magma plumbing system. In this study, our interpretation is somewhat limited by the temporal sampling after 2008. However, the launch of a new generation of SAR missions, such as Sentinel-1 (European Space Agency), will hugely improve the temporal sampling of SAR images acquired over active volcanoes, leading to a better understanding of their eruptive cycle.

Acknowledgments
The Envisat ASAR data were provided by European Space Agency through category-1 project 13248. This research was supported by French Centre National d'Etudes Spatiales (CNES). ISTerre is part of Labex OSUG@2020 (ANR10 LABX56). We thank two anonymous reviewers for their suggestions that significantly improved our manuscript as well as J.-L. Le Pennec for fruitful discussions.

The Editor thanks Pablo Samaniego and Juliet Biggsfor for their assistance in evaluating this paper.

References

Arellano, S., M. Hall, P. Samaniego, J.-L. L. Pennec, A. Ruiz, I. Molina, and H. Yepes (2008), Degassing patterns of Tungurahua volcano (Ecuador) during the 1999–2006 eruptive period, inferred from remote spectroscopic measurements of SO_2 emissions, *J. Volcanol. Geotherm. Res.*, *176*(1), 151–162, doi:10.1016/j.jvolgeores.2008.07.007.

Bagnardi, M., and F. Amelung (2012), Space-geodetic evidence for multiple magma reservoirs and subvolcanic lateral intrusions at Fernandina Volcano, Galapagos Islands, *J. Geophys. Res.*, *117*, B10406, doi:10.1029/2012JB009465.

Biggs, J., P. Mothes, M. Ruiz, F. Amelung, T. H. Dixon, S. Baker, and S. H. Hong (2010), Stratovolcano growth by co-eruptive intrusion: The 2008 eruption of Tungurahua Ecuador, *Geophys. Res. Lett.*, *37*, L21302, doi:10.1029/2010GL044942.

Crisp, J. A. (1984), Rates of magma emplacement and volcanic output, *J. Volcanol. Geotherm. Res.*, *20*(3–4), 177–211.

Delgado, F., M. Pritchard, R. Lohman, and J. Naranjo (2014), The 2011 Hudson volcano eruption (Southern Andes, Xhile): Pre-eruptive inflation and hotspots observed with InSAR and thermal imagery, *Bull. Volcanol.*, *76*(5), 1–19.
Dzurisin, D. (2003), A comprehensive approach to monitoring volcano deformation as a window on the eruption cycle, *Rev. Geophys.*, *41*(2), 1009, doi:10.1029/2003RG000134.
Efron, B., and R. Tibshirani (1986), Bootstrap methods for standard errors, confidence intervals, and other measures of statistical accuracy, *Stat. Sci.*, *1*, 54-75.
Elsworth, D., G. Mattioli, J. Taron, B. Voight, and R. Herd (2008), Implications of magma transfer between multiple reservoirs on eruption cycling, *Science*, *322*, 246–248.
Eychenne, J., J.-L. Pennec, L. Troncoso, M. Gouhier, and J.-M. Nedelec (2012), Causes and consequences of bimodal grain-size distribution of tephra fall deposited during the August 2006 Tungurahua eruption (Ecuador), *Bull. Volcanol.*, *74*(1), 187–205.
Eychenne, J., J.-L. Le Pennec, P. Ramón, and H. Yepes (2013), Dynamics of explosive paroxysms at open-vent andesitic systems: High-resolution mass distribution analyses of the 2006 Tungurahua fall deposit (Ecuador), *Earth Planet. Sci. Lett.*, *361*, 343–355.
Farr, T. G., et al. (2007), The shuttle radar topography mission, *Rev. Geophys.*, *45*, RG2004, doi:10.1029/2005RG000183.
Feigl, K. L., H. Le Mével, S. Tabrez Ali, L. Córdova, N. L. Andersen, C. DeMets, and B. S. Singer (2014), Rapid uplift in Laguna del Maule volcanic field of the Andean Southern Volcanic zone (Chile) 2007–2012, *Geophys. J. Int.*, *196*(2), 885–901.
Ferretti, A., C. Prati, and F. Rocca (2001), Permanent scatterers in SAR interferometry, *IEEE Trans. Geosci. Remote Sens.*, *39*(1), 8–20.
Fialko, Y., and J. Pearse (2012), Sombrero uplift above the Altiplano-Puna magma body: Evidence of a ballooning mid-crustal diapir, *Science*, *338*(6104), 250–252, doi:10.1126/science.1226358.
Foroozan, R., D. Elsworth, B. Voight, and G. S. Mattioli (2010), Dual reservoir structure at Soufrière Hills Volcano inferred from continuous GPS observations and heterogeneous elastic modeling, *Geophys. Res. Lett.*, *37*, L00E12, doi:10.1029/2010GL042511.
Fournier, T. J., M. E. Pritchard, and S. N. Riddick (2010), Duration, magnitude, and frequency of subaerial volcano deformation events: New results from Latin America using InSAR and a global synthesis, *Geochem. Geophys. Geosyst.*, *11*, Q01003, doi:10.1029/2009GC002558.
Froger, J. L., D. Remy, S. Bonvalot, and D. Legrand (2007), Two scales of inflation at Lastarria-Cordon del Azufre volcanic complex, central Andes, revealed from ASAR-ENVISAT interferometric data, *Earth Planet. Sci. Lett.*, *255*(1–2), 148–163.
Hall, M. L., A. L. Steele, P. A. Mothes, and M. C. Ruiz (2013), Pyroclastic density currents (PDC) of the 16–17 August 2006 eruptions of Tungurahua volcano, Ecuador: Geophysical registry and characteristics, *J. Volcanol. Geotherm. Res.*, *265*, 78–93.
Hall, M. L., C. Robin, B. Beate, P. Mothes, and M. Monzier (1999), Tungurahua Volcano, Ecuador: Structure, eruptive history and hazards, *J. Volcanol. Geotherm. Res.*, *91*(1), 1–21.
Henderson, S. T., and M. E. Pritchard (2013), Decadal volcanic deformation in the Central Andes Volcanic Zone revealed by InSAR time series, *Geochem. Geophys. Geosyst.*, *14*, 1358–1374, doi:10.1002/ggge.20074.
Hooper, A., P. Segall, and H. Zebker (2007), Persistent scatterer interferometric synthetic aperture radar for crustal deformation analysis, with application to Volcán Alcedo, galápagos, *J. Geophys. Res.*, *112*, B07407, doi:10.1029/2006JB004763.
Hooper, A., F. Prata, and F. Sigmundsson (2012a), Remote sensing of volcanic hazards and their precursors, *Proc. IEEE*, *100*(10), 2908–2930.
Hooper, A., D. Bekaert, K. Spaans, and M. Arikan (2012b), Recent advances in SAR interferometry time series analysis for measuring crustal deformation, *Tectonophysics*, *514-517*, 1–13.
Kelfoun, K., P. Samaniego, P. Palacios, and D. Barba (2009), Testing the suitability of frictional behaviour for pyroclastic flow simulation by comparison with a well-constrained eruption at Tungurahua volcano (Ecuador), *Bull. Volcanol.*, *71*(9), 1057–1075.
Le Pennec, J. L., D. Jaya, P. Samaniego, P. Ramón, S. Moreno Yánez, J. Egred, and J. van der Plicht (2008), The AD 1300–1700 eruptive periods at Tungurahua volcano, Ecuador, revealed by historical narratives, stratigraphy and radiocarbon dating, *J. Volcanol. Geotherm. Res.*, *176*(1), 70–81.
Mogi, K. (1958), Relations between the eruptions of various volcanoes and the deformations of the ground surfaces around them, *Bull. Earthquake Res. Inst.*, *36*(2), 99–134.
Molina, I., H. Kumagai, J.-L. Le Pennec, and M. Hall (2005), Three-dimensional P-wave velocity structure of Tungurahua Volcano, Ecuador, *J. Volcanol. Geotherm. Res.*, *147*(1–2), 144–156.
Mothes, P. A., M. Lisowski, M. C. Ruiz, A. Ruiz, and P. B. Palacios Palacios (2010), Borehole tiltmeter and CGPS response to VLP seismic events under Cotopaxi volcano, Ecuador, Abstract G23C-0848 presented at 2010 Fall Meeting, AGU, San Francisco, Calif., 13-17 Dec.
Ordóñez, V. M. I., and G. C. A. Rey (1997), Deformation associated with the extrusion of a dome at Galeras volcano, Colombia, 1990–1991, *J. Volcanol. Geotherm. Res.*, *77*(1–4), 115–120.
Parks, M. M., J. Biggs, T. A. Mather, D. M. Pyle, F. Amelung, M. L. Monsalve, and L. N. Medina (2011), Co-eruptive subsidence at Galeras identified during an InSAR survey of Colombian volcanoes (2006–2009), *J. Volcanol. Geotherm. Res.*, *202*(3–4), 228–240.
Pinel, V., A. Hooper, S. De la Cruz-Reyna, G. Reyes-Davila, M.-P. Doin, and P. Bascou (2011), The challenging retrieval of the displacement field from InSAR data for andesitic stratovolcanoes: Case study of Popocatepetl and Colima Volcano, Mexico, *J. Volcanol. Geotherm. Res.*, *200*, 49–61, doi:10.1016/j.jvolgeores.2010.12.002.
Pritchard, M. E., and M. Simons (2002), A satellite geodetic survey of large-scale deformation of volcanic centres in the central Andes, *Nature*, *418*, 167–171.
Reverso, T., J. Vandemeulebrouck, F. Jouanne, V. Pinel, T. Villemin, E. Sturkell, and P. Bascou (2014), A two-magma chamber model as a source of deformation at Grì-msvötn Volcano, Iceland, *J. Geophys. Res. Solid Earth*, *119*, 4666–4683, doi:10.1002/2013JB010569.
Rivalta, E., and P. Segall (2008), Magma compressibility and the missing source for some dike intrusions, *Geophys. Res. Lett.*, *35*, L04306, doi:10.1029/2007GL032521.
Rosen, P. A., S. Henley, G. Peltzer, and M. Simons (2004), Updated repeat orbit interferometry package released, *Eos Trans. AGU*, *85*(5), 47, doi:10.1029/2004EO050004.
Ruiz, M., J. Lees, and J. Johnson (2006), Source constraints of Tungurahua volcano explosion events, *Bull. Volcanol.*, *68*(5), 480–490.
Samaniego, P., J.-L. Le Pennec, C. Robin, and S. Hidalgo (2011), Petrological analysis of the pre-eruptive magmatic process prior to the 2006 explosive eruptions at Tungurahua volcano (Ecuador), *J. Volcanol. Geotherm. Res.*, *199*(1–2), 69–84.
Sparks, R. S. J., C. B. Folkes, M. C. Humphreys, D. N. Barfod, J. Clavero, M. C. Sunagua, S. R. McNutt, and M. E. Pritchard (2008), Uturuncu volcano, Bolivia: Volcanic unrest due to mid-crustal magma intrusion, *Am. J. Sci.*, *308*(6), 727–769.
Stevens, N. F., and G. Wadge (2004), Towards operational repeat-pass SAR interferometry at active volcanoes, *Nat. Hazard*, *33*(1), 47–76.
Walter, T. R., and M. Motagh (2014), Deflation and inflation of a large magma body beneath Uturuncu volcano, Bolivia? Insights from InSAR data, surface lineaments and stress modelling, *Geophys. J. Int.*, doi:10.1093/gji/ggu080.
Zebker, H., and J. Villasenor (1992), Decorrelation in interferometric radar echoes, *IEEE Trans. Geosci. Remote Sens.*, *30*, 950–959.